Voltage Sensor Movement and cAMP Binding Allosterically Regulate an Inherently Voltage-independent Closed–Open Transition in HCN Channels

Shan Chen,[1,2] Jing Wang,[1] Lei Zhou,[1] Meena S. George,[1] and Steven A. Siegelbaum[1,2,3]

[1]Center for Neurobiology and Behavior, [2]Department of Pharmacology, and [3]Howard Hughes Medical Institute, Columbia University, New York, NY 10032

The hyperpolarization-activated cyclic nucleotide-modulated cation (HCN) channels are regulated by both membrane voltage and the binding of cyclic nucleotides to a cytoplasmic, C-terminal cyclic nucleotide-binding domain (CNBD). Here we have addressed the mechanism of this dual regulation for HCN2 channels, which activate with slow kinetics that are strongly accelerated by cAMP, and HCN1 channels, which activate with rapid kinetics that are weakly enhanced by cAMP. Surprisingly, we find that the rate of opening of HCN2 approaches a maximal value with extreme hyperpolarization, indicating the presence of a voltage-independent kinetic step in the opening process that becomes rate limiting at very negative potentials. cAMP binding enhances the rate of this voltage-independent opening step. In contrast, the rate of opening of HCN1 is much greater than that of HCN2 and does not saturate with increasing hyperpolarization over the voltage range examined. Domain-swapping chimeras between HCN1 and HCN2 reveal that the S4–S6 transmembrane region largely determines the limiting rate in opening kinetics at negative voltages. Measurements of HCN2 tail current kinetics also reveal a voltage-independent closing step that becomes rate limiting at positive voltages; the rate of this closing step is decreased by cAMP. These results are consistent with a cyclic allosteric model in which a closed–open transition that is inherently voltage independent is subject to dual allosteric regulation by voltage sensor movement and cAMP binding. This mechanism accounts for several properties of HCN channel gating and has potentially important physiological implications.

INTRODUCTION

The HCN gene family (HCN1–4) encodes nonselective cation channels that are activated by membrane hyperpolarization and directly regulated by cyclic nucleotides (Biel et al., 2002; Robinson and Siegelbaum, 2003; Baruscotti et al., 2005). These channels underlie the hyperpolarization-activated current (I_f or I_h) that contributes to pacemaking activity in both heart and brain. Binding of cAMP or cGMP to a C-terminal cyclic nucleotide-binding domain (CNBD) enhances channel opening by speeding the rate of opening and shifting the relation between opening and membrane hyperpolarization to more positive potentials (DiFrancesco and Tortora, 1991). Although previous studies have identified domains of HCN channels that are important for both cyclic nucleotide-dependent regulation (Viscomi et al., 2001; Wainger et al., 2001; Wang et al., 2001; Zagotta et al., 2003) and voltage gating (Chen et al., 2000; Vaca et al., 2000; Mannikko et al., 2002; Bell et al., 2004; Vemana et al., 2004), the mechanism coupling voltage sensor movement, ligand binding, and channel opening remains unclear.

A number of kinetic models have been proposed to account for the voltage-dependent gating and cyclic nucleotide-dependent modulation of the HCN channels (DiFrancesco, 1999; Altomare et al., 2001; Wang et al., 2002; Craven and Zagotta, 2004; Shin et al., 2004; Mannikko et al., 2005). One unresolved question is whether voltage sensor movement directly opens the channel (DiFrancesco, 1999; Wang et al., 2002; Mannikko et al., 2005), as it does in a Hodgkin-Huxley model (Hodgkin and Huxley, 1952), or whether opening occurs through a reaction that is distinct from voltage sensor movement. Evidence that the final transition that opens the channel is inherently voltage independent, and thus distinct from voltage sensor movement, comes from the finding that cAMP, in addition to shifting voltage gating to more positive potentials, increases the maximal open probability of the channel at extreme hyperpolarized voltages, where voltage-dependent gating has reached completion (Craven and Zagotta, 2004; Shin et al., 2004). If opening itself were voltage dependent, then the channel should be fully opened at such negative voltages and thus immune to any further increase in opening with cAMP.

Correspondence to Steven A. Siegelbaum: sas8@columbia.edu

J. Wang's present address is Department of Anesthesiology, Columbia University Medical Center, 630 W. 168 St., New York, NY 10032.

S. Chen's present address is Department of Medicine, Flushing Hospital Medical Center, 4500 Parson's Blvd., Flushing, NY 11355.

Abbreviations used in this paper: CNBD, cyclic nucleotide-binding domain; EPSP, excitatory postsynaptic potential; HCN, hyperpolarization-activated cyclic nucleotide-modulated cation.

J. Gen. Physiol. © The Rockefeller University Press $15.00
Volume 129 Number 2 February 2007 175–188
http://www.jgp.org/cgi/doi/10.1085/jgp.200609585

Supplemental Material can be found at:
http://www.jgp.org/cgi/content/full/jgp.200609585/DC1

These effects of cAMP have been modeled by reaction schemes in which channels undergo a voltage-dependent activation reaction followed by a voltage-independent opening step that is enhanced by cAMP binding (Craven and Zagotta, 2004; Shin et al., 2004). Such models predict that the rate of HCN channel opening and closing should become voltage independent at extreme negative or positive voltages, respectively, where the voltage-independent rates of channel opening and closing become rate limiting. Here we demonstrate such voltage-independent kinetic properties for the gating of HCN2. Moreover, we find that cAMP enhances the voltage-independent rate of channel opening and slows the voltage-independent rate of channel closing. Such results are consistent with an eight-state cyclic allosteric scheme in which voltage gating and cAMP binding independently regulate a closed–open transition that is inherently voltage independent. In contrast, the rate of opening of HCN1 does not reach a voltage-independent maximum, indicating that its closed–open transition has faster inherent kinetics than that of HCN2, and so does not become rate limiting over the voltage range examined. Chimera studies reveal that the differences in the rate of the voltage-independent opening step between HCN1 and HCN2 are largely localized to the S4–S6 transmembrane region. The presence of a rate-limiting voltage-independent step in both channel opening and closing may serve an important physiological function by preventing channel kinetics from becoming excessively rapid at extreme negative or positive potentials.

MATERIALS AND METHODS

Molecular Biology

Mouse HCN1 (Santoro et al., 1998) and HCN2 (Ludwig et al., 1998) were subcloned into the *pGH19* and *pGHE* expression vectors, respectively (Santoro et al., 2000; Chen et al., 2001). Deletion mutants and chimeras were made by a PCR/subcloning strategy, and the resulting mutant HCN channels were verified by dideoxy chain termination sequencing.

In one series of chimeras, we exchanged the entire cytoplasmic N terminus, the S1–S6 core transmembrane domain, or the cytoplasmic C terminus between HCN1 and HCN2 (Wang et al., 2001). We identify such chimeras using the nomenclature XYZ, where X, Y, or Z is a number, either 1 or 2, that refers to the HCN isoform encoding the N terminus, core transmembrane domain, or C terminus, respectively (see cartoons in figures). In a second series of chimeras, we subdivided the S1–S6 transmembrane domain into two subregions: the S1–S3 region and the S4–S6 region. We refer to these chimeras as $XY_{SZ}X$, where X refers to the parent channel (HCN1 or HCN2), Y refers to the identity of the donor channel from which the subregion was derived, and SZ refers to the subregion that has been replaced (that is, either S1–3 or S4–6) (see Fig. 4). In $21_{S1\text{-}3}2$, S1–S3 of HCN2 (residues D182–E282) was replaced by S1–S3 of HCN1 (D129–E229). In $21_{S4\text{-}6}2$, S4–S6 (including the S3–S4 linker) of HCN2 (K283–L442) was replaced by S4–S6 of HCN1 (K230-L389). Conversely, in $12_{S1\text{-}3}1$, S1–S3 of HCN1 (D129–E229) was replaced by S1–S3 of HCN2 (D182–E282). In $12_{S4\text{-}6}1$, S4–S6 of HCN1 (K230–L389) was replaced by S4–S6 of HCN2 (K283–L442).

Expression in *Xenopus* Oocytes

cRNA was transcribed from NheI-linearized DNA (for HCN1 and mutants having the N terminus of HCN1) or SphI-linearized DNA (for HCN2 and mutants having the N terminus of HCN2) using a T7 RNA polymerase (Message Machine; Ambion). 50 ng of cRNA was injected into *Xenopus* oocytes as described previously (Goulding et al., 1992).

Electrophysiological Recordings

Cell-free inside-out patches were obtained 3–6 d after cRNA injection, and data were acquired using an Axopatch 200A patch-clamp amplifier (Axon Instruments). A symmetrical recording solution was used on both sides of the membrane, containing (in mM) 107 KCl, 5 NaCl, 10 HEPES, 1 $MgCl_2$, and 1 EGTA, pH 7.3. Patch pipettes had resistances of 1–3 MΩ and were coated with Sylgard to minimize capacitance. An Ag-AgCl ground wire was connected to the bath solution by a 3 M KCl agar bridge, and junction potential was compensated before the formation of each patch. Channel opening kinetics were measured using hyperpolarizing voltage pulses applied to inside-out patches in −10-mV step increments from the holding potential −40 mV. Channel closing kinetics were measured by stepping the membrane to a negative voltage to activate the channel, and then returning the voltage to a series of more positive steps, also in −10-mV increments. All recordings were obtained at room temperature (22–25°C). Leak current was not subtracted. Data were filtered at 1 kHz with the Axopatch 200A built-in 4-pole, low-pass Bessel filter and sampled at 2 kHz with an ITC-18 analogue-to-digital interface. Analysis was done using PulseFit, IgorPro, and Sigma Plot. All steady-state activation data included in this paper were obtained after the $V_{1/2}$ measurements had stabilized following patch excision (Chen et al., 2001).

Data Analysis

Current records during hyperpolarizing voltage steps were fit with a single exponential function, $I = I_{ss}(1 - \exp[-t/\tau])$, after an initial delay (Wainger et al., 2001). I_{ss} represents the steady-state current, and τ represents the time constant. Steady-state activation curves were measured by plotting the peak tail current amplitude measured on return to the holding potential of −40 mV after hyperpolarizing steps to different test voltages as previously described (Wang et al., 2001). The activation curves were fit with a modified Boltzmann equation: $I_{tail}(V) = A_1 + A_2/\{1 + \exp[(V - V_{1/2})/s]\}$, where A_1 is an offset caused by a non-zero holding current, A_2 is the maximal tail current amplitude, V is voltage during the hyperpolarizing test pulse, $V_{1/2}$ is the midpoint activation voltage, and s is the slope factor of the relation (in mV). The peak tail current amplitudes were converted to a normalized Hodgkin-Huxley activation variable, f_∞, that varied from 0 to 1, by subtracting A_1 from $I_{tail}(V)$ and dividing by A_2.

To reduce variability due to slight shifts in the voltage dependence of opening between experiments (standard errors for $V_{1/2}$ values <2 mV), we plotted values of $1/\tau$ versus membrane voltage relative to the $V_{1/2}$ determined for each individual experiment (determined by subtracting the $V_{1/2}$ from the test voltage during the hyperpolarization). Kinetic data from multiple experiments were grouped based on relative voltage in bins between V' and V' + ΔV mV, where V' is the relative voltage and ΔV is the bin size (~5 mV). Kinetic values within a given voltage bin were then averaged. We then converted the relative voltage back to an absolute voltage by adding the mean $V_{1/2}$ obtained from all experiments to the relative voltage. Each $1/\tau$ value was associated with a standard error in both the $1/\tau$ axis and voltage axis; these errors are shown in the plots (when the error bar was larger than the symbol). As seen from the horizontal error bars in the plots, the corrections for voltage shifts were small.

Tail current kinetics were measured by stepping the membrane to depolarized voltages following a constant hyperpolarizing step

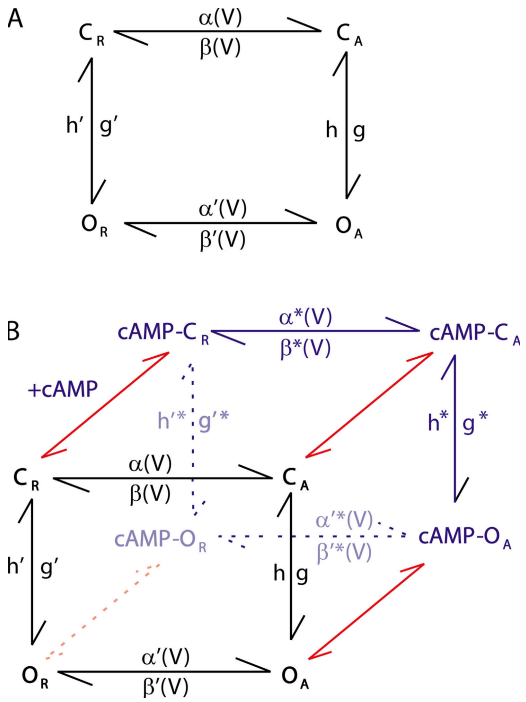

Figure 1. Four-state and eight-state allosteric models for regulation of HCN2 opening by voltage and cAMP. (A) The four-state cyclic allosteric scheme for channel opening in the absence of cAMP. The vertical transitions represent the voltage-independent opening and closing reactions. The horizontal transitions are voltage-dependent activation steps that reflect voltage sensor movements. α and β are the voltage-dependent rate constants for activation and deactivation, respectively, for the closed state of the channel. α′ and β′ are the voltage-dependent rate constants for activation and deactivation, respectively, for the open state of the channel. g and h are the rate constants for opening and closing, respectively, for the activated state of the channel. g′ and h′ are the rate constants for opening and closing, respectively, for the resting state of the channel. (B) The eight-state cubic scheme for the regulatory effects of both cAMP and voltage on channel opening. The four unliganded states correspond to the vertices on the front face of the cube (in black), and undergo transitions identical to those shown in A. The four cAMP-bound states form the four vertices on the back face of the cube (in blue). Rate constants marked with asterisks are for the cAMP-bound state transitions. In general, these rate constants differ from those in the absence of ligand. Ligand binding (+cAMP) and unbinding steps are shown in red. Transitions and states lying on hidden edges and corners of the cube are drawn with dashed lines and lighter shades. The rate constants for the binding and unbinding reactions are not shown since these transitions do not occur under the conditions of our experiments, performed in either the absence of cAMP or a saturating concentration of ligand.

to open the channels. Tail currents were then fit by a single exponential function, $I = I_0\exp(-t/\tau)$, following an initial delay, and the rate of closing ($1/\tau$) was plotted.

Modeling HCN2 Gating by Voltage and cAMP

Data Normalization. To fit different kinetic models to our data, we converted our experimental HCN currents to a normalized, Hodgkin-Huxley activation variable, $f(t)$. Currents recorded during channel opening in response to hyperpolarization were transformed using the following equation: $f(t) = [I(t)/Iss]\cdot f_\infty$, where $I(t)$ is the leak-subtracted current during a hyperpolarization at time t, Iss is the steady-state leak-subtracted current at the end of the pulse, and f_∞ is the steady-state activation variable obtained from tail current activation curves. Because f_∞ is a normalized activation variable and not a true open probability, $f(t)$ is also a normalized quantity. We converted experimental tail current measurements into normalized $f(t)$ values by subtracting the steady-state tail current value from the time-dependent tail current at each potential. We then divided this result by its peak value measured 10–20 ms after the end of the hyperpolarization. In the fits of the models to the data, we converted the true open probabilities calculated from the models (fractional occupancy of open state[s]) into normalized values using a procedure corresponding to the above experimental normalization protocols.

Three-State Scheme. We initially fit HCN2 currents by a three-state kinetic reaction mechanism in which gating proceeds through two sequential closed states (C_R and C_A) followed by a transition to a single open state (O_A):

$$C_R \underset{\beta(V)}{\overset{\alpha(V)}{\rightleftharpoons}} C_A \underset{h}{\overset{g}{\rightleftharpoons}} O_A \qquad (1)$$

The transition between the two closed states was assumed to be voltage dependent, reflecting the movement of the voltage sensor between its resting (R) and activated (A) conformations, where $\alpha(V)$ and $\beta(V)$ are the voltage-dependent rate constants of activation and deactivation, respectively. The transition between the closed activated state (C_A) and the open state (O_A) was assumed to be voltage independent, where g and h are the voltage-independent rate constants of opening and closing, respectively. We also assumed that the rate constants for the voltage-dependent reaction depend exponentially on membrane potential according to $\alpha(V) = \alpha_0\exp(-V/s_\alpha)$ and $\beta(V) = \beta_0\exp(V/s_\beta)$, where α_0 and β_0 are the rate constants at 0 mV and s_α and s_β are the voltage-dependent slope factors in units of mV. Thus, the model of Eq. 1 has a total of six free parameters (α_0, s_α, β_0, s_β, g, and h).

We used a nonlinear least-squares global fitting routine in NEURON's Multiple Run Fitter (NEURON version 5.8, available at http://www.neuron.yale.edu/neuron) to obtain the best fit of the above reaction scheme to a set of $f(t)$ traces for steps to a series of hyperpolarizations.

Four-State and Eight-State Schemes. We next fit our opening and tail current data in the absence of cAMP by a four-state cyclic allosteric scheme (Fig. 1 A), which is described in more detail in Results. In this scheme, channels undergo a voltage-dependent activation reaction ($C_R \leftrightarrow C_A$) followed by a voltage- independent opening step ($C_A \leftrightarrow O_A$), as in the three-state linear model. However, closed resting channels (C_R) additionally can open directly into an open resting state, O_R, by a second voltage-independent reaction that occurs when the voltage sensors are in the resting position ($C_R \leftrightarrow O_R$). g′ and h′ are the voltage-independent rate constants for opening and closing, respectively, through this pathway. Because this is a cyclic scheme, voltage sensor movement also occurs between the open resting (O_R) and open activated (O_A) states ($O_R \leftrightarrow O_A$), where α′ (V) and β′ (V) are the rate constants for voltage sensor activation and deactivation, respectively, for the open states of the channel.

To model the action of cAMP, we assumed that ligand can bind to all four states of the cyclic scheme. This results in an eight-state cubic scheme, with the vertices of the front face of the cube corresponding to the four unliganded states and the vertices of the back face of the cube corresponding to the four liganded states (Fig. 1 B). However, since we only studied channel behavior in either the absence of cAMP (four unliganded states only) or in the presence of a saturating concentration of cAMP (four liganded states only), we fit the data obtained in the absence or presence

TABLE I

Four-State and Eight-State Model Kinetic Parameters

	Separate four-state scheme fits		Single eight-state scheme fit	
Parameters	0 cAMP	10 μM cAMP	0 cAMP	10 μM cAMP
α_0 (ms^{-1})	3.2×10^{-6} (1.0×10^{-6} to 1.0×10^{-5})	1.3×10^{-7} (8.0×10^{-8} to 1.9×10^{-7})	3.9×10^{-6} (1.5×10^{-7} to 4.0×10^{-5})	
s_α (mV)	9.1 (8 to 17)	9.6 (9.2 to 10)	8.0 (5.9 to 12.5)	
β_0 (ms^{-1})	415.8 (200 to 900)	1042.7 (850 to 1440)	5040.6 (30 to 9200000)	
s_β (mV)	49.0 (20 to 150)	13.6 (13.4 to 13.9)	46.1 (14.3 to 1666.7)	
g (ms^{-1})	0.0024 (0.0012 to 0.0045)	0.0036 (0.0025 to 0.004)	0.0017 (0.0003 to 0.0046)	0.011 (0.0037 to 0.039)
h (ms^{-1})	3.8×10^{-4} (3.0 to 5.0×10^{-4})	1.5×10^{-4} (1.1 to 2.5×10^{-4})	4.3×10^{-4} (2.0 to 9.0×10^{-4})	1.4×10^{-4} (3.8×10^{-5} to 2.8×10^{-4})
α_0' (ms^{-1})	1.1×10^{-5} (see below)	1.7×10^{-6} (see below)	1.3×10^{-5} (4.0×10^{-7} to 9.0×10^{-5})	
s_α' (mV)	9.9 (see below)	6.9 (see below)	8.3 (see below)	
β_0' (ms^{-1})	0.045 (0.026 to 0.09)	0.055 (0.027 to 0.14)	0.050 (0.02 to 0.14)	
s_β' (mV)	33.9 (22.2 to 57.1)	29.7 (17.5 to 50)	32.6 (18.2 to 66.7)	
g' (ms^{-1})	4.2×10^{-6} (4×10^{-7} to 6.8×10^{-5})	1.6×10^{-6} (1.3×10^{-7} to 2.6×10^{-5})	2.5×10^{-7} (see below)	3.9×10^{-6} (see below)
h' (ms^{-1})	0.021 (0.017 to 0.032)	0.016 (0.0135 to 0.022)	0.020 (0.016 to 0.036)	0.017 (0.013 to 0.028)
Sum-squared error	0.0080	0.0079	0.0103	0.0112

Parameters from separate four-state fits to data in Fig. 8 B (0 cAMP, four-state column) and Fig. 8 C (10 μM cAMP, four-state column), and for fits of eight-state scheme to data in Fig. S1 A (0 cAMP, eight-state column) and S1 B (10 μM cAMP, eight-state column). Lower and upper ranges for each parameter are given in parentheses (see Materials and methods). For eight-state fits, parameters for voltage-independent rates shown in absence (lefthand cells) or presence of cAMP (righthand cells). Parameters for all voltage-dependent rates were identical in presence or absence of cAMP. For parameters computed by microscopic reversibility constraints, the parameter range is not listed.

of cAMP by the two appropriate four-state schemes. In an unconstrained version of the fit (Fig. 8 C), cAMP binding was allowed to modulate all transitions. In a constrained version of the fit, we assumed that cAMP binding only modulates the two voltage-independent closed–open transitions (Fig. S1, available at http://www.jgp.org/cgi/content/full/jgp.200609585/DC1). This latter scheme corresponds to an eight-state model in which both voltage sensor movement and cAMP binding independently modulate the closed–open transition. Because the experimental data were obtained in either the absence of cAMP or the presence of a saturating concentration of ligand, transitions between the unbound and cAMP-bound states were not allowed in the model. The open probabilities calculated by the model (summed probability of fractional occupancy of O_R and O_A) were appropriately normalized to allow comparison with the normalized experimental $f(t)$ values.

We used the NEURON global fitting routine to obtain the best combined fit to a set of opening traces and an independent set of tail current closing traces. The best-fit parameter values and least sum-squared errors are given in Table I. The indicated total error for each model is the sum over all traces (both opening and closing traces) of the mean squared error (between the model and the data) for each trace for the best-fit set of parameter values. Parameter ranges were computed by perturbing the value of each parameter, one at a time, to a new fixed value. We then reran the fitting routine, allowing all other parameters to vary to obtain the best fit with the perturbed, fixed parameter value. The perturbation was increased until the total mean error for a given scheme had increased above the total error for the initial set of best fit parameters by ~25–30%, a value that yielded a noticeable deterioration in the quality of the fits as judged by eye. The resultant parameter ranges were more than an order of magnitude larger than the 95% confidence intervals reported by the nonlinear least-squares fitting routine of the Igor software package (based on the covariance matrix associated with the Levenberg-Marquardt fitting method in Press et al., 1992). Thus, our parameter intervals probably provide an upper limit of the likely range in which the "true" parameter values lie.

Online Supplemental Material

Additional modeling results (available online at http://www.jgp.org/cgi/content/full/jgp.200609585/DC1) show the results of fitting HCN2 opening and tail current data in the absence and presence of cAMP using an eight-state cyclic allosteric model in which cAMP binding was assumed to selectively alter the voltage-independent closed−open transition (Fig. S1).

RESULTS

Differences in Opening Kinetics between HCN1 and HCN2

Both HCN1 and HCN2 channels open in response to hyperpolarizing voltage steps, with the opening kinetics of HCN1 being much more rapid that those of HCN2 (Fig. 2 A), as previously described (Santoro et al., 2000; Chen et al., 2001; Wainger et al., 2001; Wang et al., 2001). The opening kinetics for both HCN1 and HCN2 are described reasonably well by a single exponential function (with time constant τ) following a brief delay. The rate of opening ($1/\tau$) increases with increasing hyperpolarization for both channels, with HCN2 opening rates being 5–10-fold slower than those of HCN1 over a wide range of voltages (Fig. 2 B and Santoro et al., 2000). By extending the range of hyperpolarizing voltages beyond that previously characterized, we now report a novel distinction between HCN1 and HCN2.

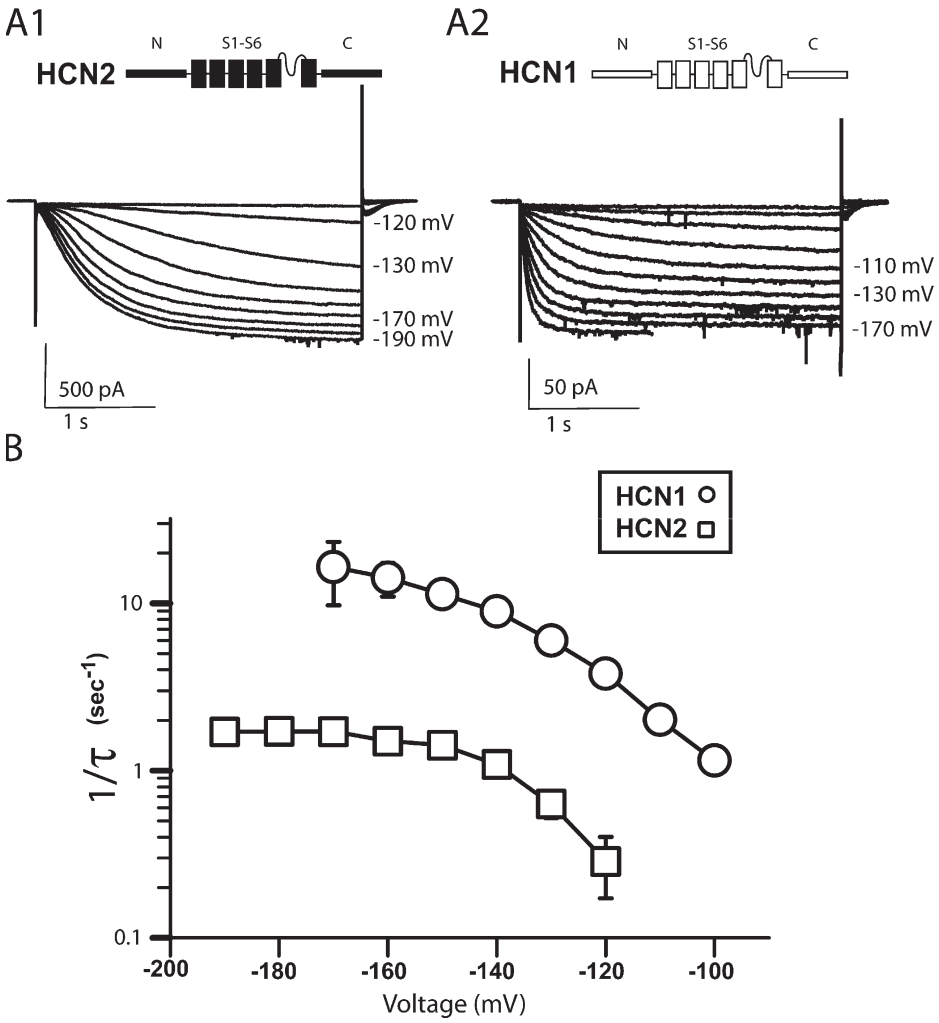

Figure 2. Kinetics of HCN2 and HCN1 opening over a wide range of hyperpolarized voltages. (A1 and A2) Currents from inside-out patches obtained from oocytes injected with cRNA of HCN2 (A1) or HCN1 (A2), respectively. Currents were elicited by hyperpolarizing steps 4 s in length. Patches were stepped from a holding potential of −40 mV in 10-mV hyperpolarizing increments to test potentials ranging from −90 to −190 mV for HCN2 and from −70 to −170 mV for HCN1. Icons besides the HCN symbols represent the domain structures of HCN channels (intracellular N and C termini and the S1–S6 transmembrane domain) using solid rectangles for HCN2 and open rectangles for HCN1. (B) Relation between the rate of opening (obtained from reciprocal of the time constant of opening, τ) for HCN2 (squares) and HCN1 (circles) versus hyperpolarizing test potential. Values of $1/\tau$ (units of 1/seconds) were measured by fitting the opening time course of HCN currents with a single exponential function following an initial delay. $n = 8$ for HCN1; $n = 6$ for HCN2. Standard error bars are shown when larger than the symbol. Note that we examined a slightly more restricted range of potentials for HCN1 than HCN2 due to the greater degree of patch instability at negative voltages from oocytes expressing HCN1.

Whereas the opening kinetics of HCN1 continue to get faster with increasing hyperpolarization, the rate of opening of HCN2 reaches a maximal, saturating value at extreme negative potentials.

Part of the kinetic differences between HCN1 and HCN2 can be attributed to a hyperpolarizing shift of the $1/\tau$ versus voltage relation for HCN2 compared with HCN1, similar to the shift in steady-state voltage gating between the two channels (Santoro et al., 2000). However, in addition to the voltage shift, there is a clear difference in the maximal rate of opening at negative voltages between the two channels. Thus, the rate of activation of HCN2 reaches a maximal, saturating value at voltages negative to −160 mV of $\sim 1-2\ s^{-1}$. In contrast, the rate of activation of HCN1 is 10-fold faster than that of HCN2, and does not show signs of saturating at the most negative potentials studied.

Distinct Channel Domains Regulate the Differences in Opening Kinetics between HCN1 and HCN2

To determine which channel regions are responsible for the different kinetic properties of HCN1 and HCN2, we examined a series of chimeras that was previously used to probe the differences in steady-state voltage gating and cAMP modulation between these channels (Wang et al., 2001). We first examined the importance of the N terminus, a region that was previously found to have little influence on steady-state voltage gating of HCN channels (Altomare et al., 2001; Wang et al., 2001). In agreement with these previous studies, we find that N-terminal sequence differences are also not responsible for differences in gating kinetics between HCN1 and HCN2 (Fig. 3 A). Thus, replacement of the N terminus of HCN2 with that of HCN1 yields a chimera (chimera 122; see Materials and methods for nomenclature) whose opening kinetics are similar to those of HCN2. Similarly, the opening kinetics of the converse chimera, in which we replaced the N terminus of HCN1 with that of HCN2 (chimera 211), are similar to those of HCN1.

We next studied the role of the cytoplasmic C terminus in determining the kinetic differences between HCN1 and HCN2 (Fig. 3 B). This region is responsible for much of the disparity in cAMP modulation and steady-state voltage gating between HCN1 and HCN2

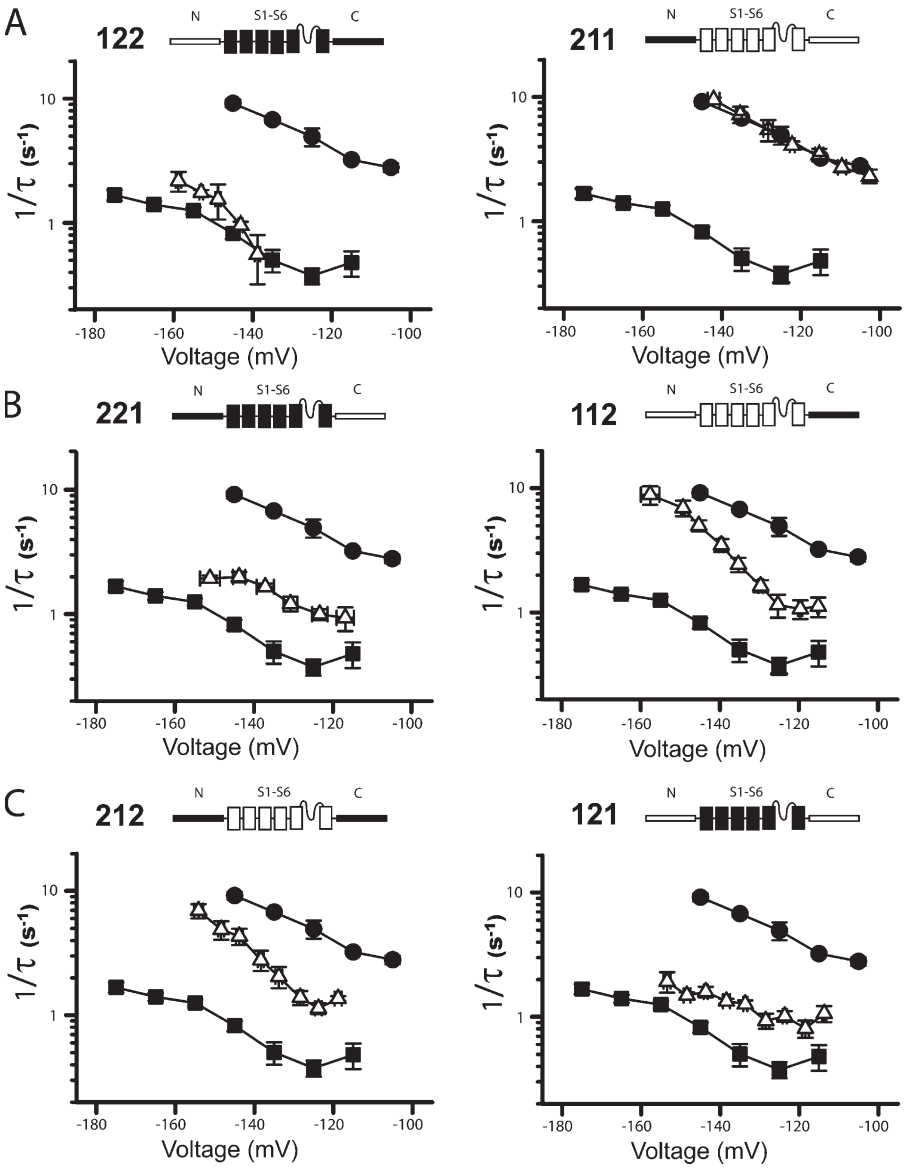

Figure 3. Role of HCN channel domains in determining the differences in opening kinetics between HCN1 and HCN2. Chimeras between wild-type HCN1 and HCN2 were made by swapping the N termini, transmembrane domains, or C termini between the two channels. Icons in each panel show approximate composition of different chimeras. Filled objects represent HCN2 sequences and open objects represent HCN1 sequences. Each graph plots mean binned values of $1/\tau$ as a function of normalized binned test voltage (see Materials and methods) for HCN2 (squares; $n = 9$), HCN1 (circles; $n = 7$), and given chimera (open triangles). Standard error bars are shown when larger than the symbol for both the $1/\tau$ and voltage axes (see Materials and methods). Note that HCN1 and HCN2 data in this and subsequent figures was obtained from a different series of experiments than shown in Fig. 2. (A) Chimeras in which the N terminus of HCN2 was replaced by the N terminus of HCN1 (122, left; $n = 6$) or in which the N terminus of HCN1 was replaced with the N terminus of HCN2 (211, right; $n = 7$). (B) Chimeras in which the C terminus of HCN2 was replaced by the C terminus of HCN1 (221, left; $n = 8$) or in which the C terminus of HCN1 was replaced with the C terminus of HCN2 (112, right; $n = 8$). (C) Chimeras in which the S1–S6 region of HCN2 was replaced by the corresponding region of HCN1 (212, left; $n = 7$) or in which the S1–S6 region of HCN1 was replaced with that of HCN2 (121, right; $n = 8$).

(Wang et al., 2001). Consistent with these previous results, we find that replacement of the C terminus of HCN2 with that of HCN1 generates a chimera (221) whose opening kinetics are more rapid than those of HCN2 (at least for steps to voltages positive to −150 mV). This reflects an ∼20-mV positive shift in the $1/\tau$ versus voltage relation due to the influence of the HCN1 C terminus, similar to the shift in steady-state gating seen with 221 relative to HCN2 (Wang et al., 2001). Conversely, 112 exhibits a slowing in its opening kinetics relative to HCN1 due to a hyperpolarizing shift of ∼14 mV in the relation between $1/\tau$ and voltage, comparable to the shift in the steady-state gating curve of 112 relative to HCN1 (Wang et al., 2001).

However, despite the large shifts in the voltage dependence of channel opening kinetics, the C-terminal exchanges do not affect the maximal rate of opening at extreme hyperpolarized potentials; nor do these exchanges alter the tendency of opening rates to reach a saturating, voltage-independent limit. Thus, the rate of opening of 112 continues to increase with increasing hyperpolarization, similar to HCN1, whereas the rate of opening of 221 reaches a maximum with extreme hyperpolarization that is similar to the limiting rate in HCN2. These results thus imply that the presence or absence of a voltage-independent limit to the rate of opening is controlled by the transmembrane domain of the channels.

To confirm the role of the transmembrane domain, we replaced the S1–S6 region of HCN2 with that of HCN1, generating the chimera 212 (Fig. 3 C). This mutation produces a dramatic speeding of opening kinetics relative to those of HCN2. The speeding is due in part to a positive voltage shift in the relation between opening rate and voltage. Importantly, we now also find that, at extreme hyperpolarized potentials, the rate of

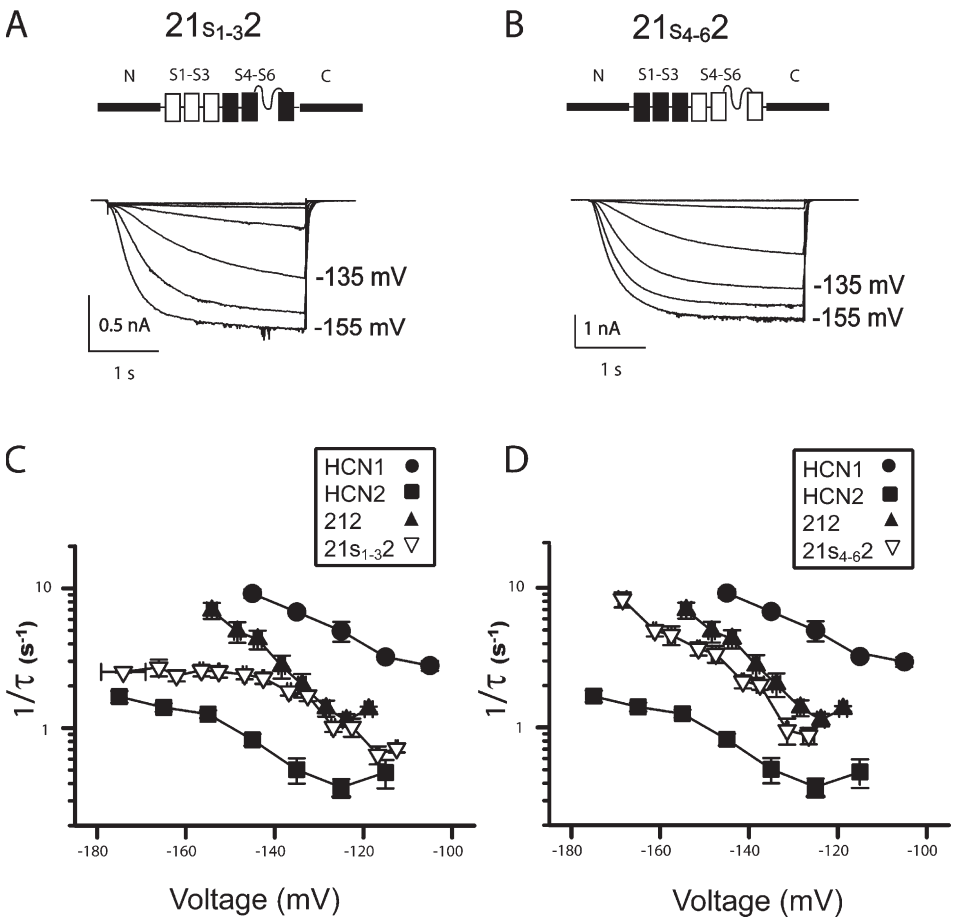

Figure 4. Effect on opening kinetics of replacing the S1–S3 or S4–S6 transmembrane subdomains of HCN2 with corresponding regions of HCN1. (A) Currents elicited by hyperpolarizing steps for chimera in which the S1–S3 region of HCN2 was replaced with the corresponding region of HCN1 (chimera $21_{S1\text{-}3}2$). (B) Currents elicited by hyperpolarizing steps for chimera in which the S4–S6 region of HCN2 was replaced with the corresponding region of HCN1 (chimera $21_{S4\text{-}6}2$). (C) Relation between the rate of opening ($1/\tau$) and test potential for the chimera $21_{S1\text{-}3}2$ (inverted open triangles; $n = 7$), chimera 212 (solid triangles, from Fig. 3 C), wild-type HCN1 (solid circles, from Fig. 3) and HCN2 (solid squares, from Fig. 3). (D) Relation between the rate of opening ($1/\tau$) and test potential for the chimera $21_{S4\text{-}6}2$ (inverted open triangles; $n = 7$) and other constructs as described above.

opening of the chimera is dramatically increased relative to HCN2 and no longer shows signs of saturating. The importance of the transmembrane domain in regulating the limiting rate of activation at negative voltages is supported by the kinetic properties of the converse chimera, 121, in which we replaced the transmembrane domain of HCN1 with that of HCN2. Relative to HCN1, 121 shows both a hyperpolarizing shift in the voltage dependence of its opening rate and a marked decrease at negative voltages in its opening rate, which now reaches a saturating maximal value, similar to the behavior of HCN2 (Fig. 3 C). Thus, whereas both the transmembrane domain and the C terminus shift the $1/\tau$ versus voltage relation along the voltage axis, the transmembrane region selectively influences the saturation behavior of the opening rate at extreme negative voltages.

The S4–S6 Subdomain Largely Determines the Limit in the Rate of Opening

Previous studies found that the S1 domain and S1–S2 extracellular linker are important determinants of the kinetic differences between HCN1 versus HCN4 (Ishii et al., 2001) and between HCN2 versus HCN4 (Stieber et al., 2003), although the issue of the voltage independence of the opening rates was not examined in these studies. Does the S1–S2 region also control the differences in gating kinetics between HCN1 and HCN2? We divided S1–S6 into two subdomains, S1–S3 and S4–S6 (the latter including the extracellular S3–S4 linker). We first replaced each of these two subdomains of HCN2 with their HCN1 counterparts (Fig. 4, A and B). This yielded one chimera, $21_{S1\text{-}3}2$, where the S1–S3 region of HCN2 was replaced by the corresponding region of HCN1, and a second chimera, $21_{S4\text{-}6}2$, where the S4–S6 region was exchanged (see Materials and methods).

The relation between $1/\tau$ and voltage for $21_{S1\text{-}3}2$ is shifted by ~20 mV in the depolarizing direction in comparison with HCN2 (Fig. 4 C). However, $1/\tau$ still reaches a saturating maximal value at extreme negative voltages that is similar to the maximal rate of opening of HCN2 and much less than the rate of opening of either HCN1 or the 212 chimera. In contrast, $21_{S4\text{-}6}2$ displays both a depolarizing shift in its $1/\tau$ versus voltage relation and, even more strikingly, a marked increase at negative potentials in its maximal rate of opening, which now no longer saturates (Fig. 4 D). Thus, $21_{S4\text{-}6}2$ largely reconstitutes the kinetic properties of 212.

Examination of the converse chimeras, $12_{S1\text{-}3}1$ and $12_{S4\text{-}6}1$, confirms the role of the S4–S6 region in determining the maximal rate of opening at negative voltages (Fig. 5). Thus, $12_{S1\text{-}3}1$ retains the characteristic properties

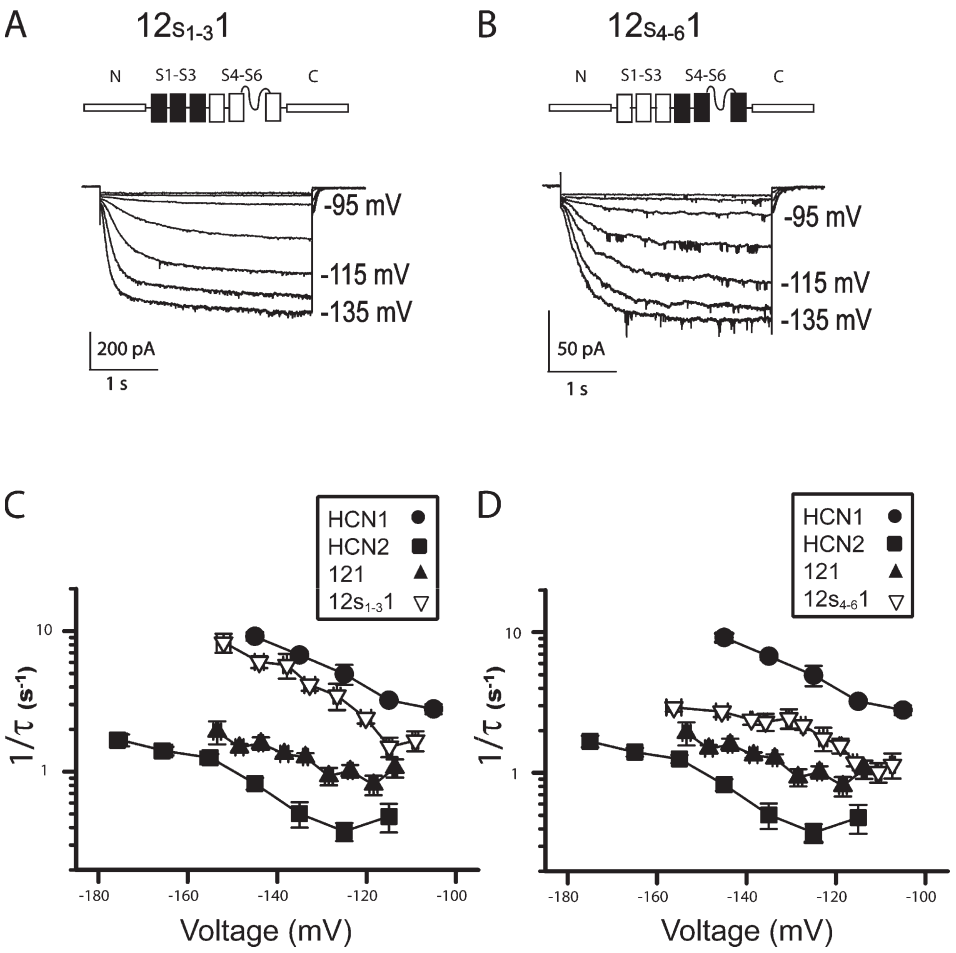

Figure 5. Effect on opening kinetics of replacing the S1–S3 or S4–S6 transmembrane subdomains of HCN1 with corresponding regions of HCN2. (A) Currents elicited by hyperpolarizing steps for chimera in which the S1–S3 region of HCN1 was replaced with the corresponding region of HCN2 (chimera $12_{S1\text{-}3}1$). (B) Currents elicited by hyperpolarizing steps for chimera in which the S4–S6 region of HCN1 was replaced with the corresponding region of HCN2 (chimera $12_{S4\text{-}6}1$). (C) Relation between the rate of opening ($1/\tau$) and test potential for the chimera $12_{S1\text{-}3}1$ (inverted open triangles; $n = 5$). $1/\tau$ values of HCN1 (filled circles), HCN2 (filled squares), and 121 (filled triangles) from Fig. 3 are also plotted for comparison. (D) Relation between the rate of opening ($1/\tau$) and test potential for the chimera $12_{S4\text{-}6}1$ (inverted open triangles; $n = 13$) and other constructs described above.

of HCN1, showing a high, nonsaturating rate of opening at negative voltages (Fig. 5, A and C), whereas $12_{S4\text{-}6}1$ behaves similarly to HCN2 and 121 in that its rate of opening saturates at a low value at negative potentials (Fig. 5, B and D). These data suggest that the identity of both the S1–S3 and S4–S6 transmembrane regions influences the position along the voltage axis of the $1/\tau$ versus voltage relation, with HCN2 sequences shifting gating to more negative potentials. In contrast, the maximal, voltage-independent rate of opening at extreme negative voltages is largely determined by the S4–S6 subdomain. We next consider the implications of this voltage-independent limit in the rate of opening for the modulatory action of cAMP on HCN2 gating.

cAMP Binding and the CNBD Regulate the Voltage-independent Rate of Opening

Previous studies have suggested that cAMP binding may enhance a voltage-independent opening step of HCN channels, based on the ability of ligand to increase the steady-state maximum open probability attained upon steps to extreme negative voltages (Shin et al., 2004; Craven and Zagotta, 2004). If this is indeed the case, cAMP application should also enhance the voltage-independent, maximal rate of opening of HCN2. In agreement with the previous studies, we find that cAMP enhances the maximal current elicited by hyperpolarizing voltages (unpublished data) and shifts the relation between the opening rate of HCN2 and voltage to more positive potentials (Fig. 6). In addition, we now report that cAMP produces a significant enhancement in the maximal, voltage-independent rate of opening of HCN2 (Fig. 6). There is a similar effect of cAMP on the chimera 122. In contrast, cAMP causes a simple depolarizing shift of the $1/\tau$ versus voltage relation for HCN1, 212, and 112, all of which contain the transmembrane domain of HCN1 and thus do not show a limiting value in their opening rate (unpublished data).

The effect of cAMP binding to enhance HCN channel opening is thought to result from the relief of a tonic inhibitory effect of the CNBD on channel opening. This conclusion is based on the finding that deletion of the CNBD produces a positive voltage shift in steady-state gating that is similar to the action of cAMP (Wainger et al., 2001). To determine whether the effect of cAMP to enhance the voltage-independent rate of opening can also be explained by a relief of C-terminal inhibition, we examined the opening kinetics of the HCN2 CNBD deletion mutant. Indeed, we find that removal of the CNBD speeds up opening in a manner

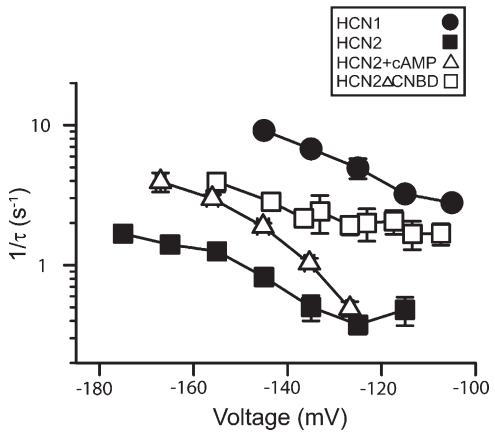

Figure 6. The effect of cAMP and deletion of the CNBD on the opening kinetics of HCN2. Rates of opening ($1/\tau$) versus test potential for HCN2 are plotted in the absence (squares) or presence (open triangles; $n = 9$) of a saturating concentration of cAMP (10 μM). Data are also shown for the HCN2ΔCNBD deletion mutant, in which the CNBD and all sequence C-terminal to the CNBD have been deleted (open squares; $n = 16$). Data for HCN1 (filled circles) are shown for comparison.

similar to that seen with cAMP, including a large increase in the maximal value of $1/\tau$ (Fig. 6).

A Three-State Model Can Account for HCN2 Opening Kinetics but not Closing Kinetics

How can we account for the voltage-independent limit to the rate of opening of HCN2 at extreme negative voltages and for the effect of cAMP to enhance this rate? These opening kinetics are not consistent with a two-state, closed–open scheme in which the rates of opening and closing monotonically increase or decrease, respectively, with increasing membrane hyperpolarization, expected for simple Eyring rate models (Hille, 2001). However, our results on opening kinetics are consistent with a simple three-state reaction scheme (Eq. 1, Materials and methods) that is similar to models proposed to explain the increase with cAMP in the maximal HCN channel open probability (Craven and Zagotta, 2004; Shin et al., 2004) or the inhibitory effects of a general anesthetic on HCN gating (Chen et al., 2005).

According to the three-state scheme, upon hyperpolarization, channels undergo a voltage-dependent transition between a closed resting state (C_R) and a closed activated state (C_A). This is followed by a voltage-independent transition to the open state (O_A) according to $C_R \leftrightarrow C_A \leftrightarrow O_A$ (see Materials and methods). The model can explain, in principle, the increase in maximal open probability with cAMP through an enhancement in the voltage-independent opening reaction. Furthermore, the model also accounts for the voltage independence of the opening rate at very negative voltages; as the membrane is increasingly hyperpolarized, the voltage-dependent activation reaction eventually becomes so rapid that the voltage-independent opening rate constant becomes limiting.

If the closed–open ($C_A \leftrightarrow O_A$) reaction is indeed voltage independent, then the voltage independent rate constant of HCN2 channel closing should also limit the rate of HCN2 tail current decay observed during steps to positive potentials following a hyperpolarizing voltage step that first opens the channels (Fig. 7). We found that the time course of the tail current is described reasonably well by a single exponential function, following an initial delay (unpublished data). A plot of the rate of tail current decay ($1/\tau$) as a function of the depolarizing step voltage shows that the decay rate initially increases as the voltage becomes more positive However, as predicted, with steps positive to 0 mV, the rate of closing reaches a maximal voltage-independent limit. In the absence of cAMP, the maximal decay rate during steps to +40 mV equals $25.4 \pm 2.7\ s^{-1}$ ($n = 4$) (Fig. 7 D). Application of cAMP decreases the rate of closing over the entire voltage range and reduces the maximal rate of closing by a factor of two (to $13.2 \pm 0.8\ s^{-1}$; $n = 4$).

To determine the adequacy of the three-state scheme to account for our kinetic data, we used a nonlinear routine to fit the model to normalized HCN2 currents activated by 10-s hyperpolarizing steps to a range of voltages (see Materials and methods). The three-state model provides a reasonable fit to the opening kinetics for HCN2 in the absence of cAMP (Fig. 8 A, left). However, there is a serious discrepancy between our experimental tail current data and the time course of tail current decay predicted by the model using the parameters obtained from the fits to the opening kinetics (Fig. 8 A, right). Thus, the maximal rate of the experimental tail current decay (around $25\ s^{-1}$) is nearly 100-fold greater than the predicted rate of tail current decay ($\sim 0.3\ s^{-1}$, see legend to Fig. 8). The disagreement between the tail current data and the predictions of the three-state model can be reconciled by a model in which HCN2 channels open and close through distinct kinetic pathways according to a four-state cyclic allosteric scheme, which we next describe.

A Four-State Cyclic Allosteric Model Accounts for both HCN2 Opening and Closing Kinetics

According to the four-state cyclic model (see Materials and methods, Fig. 1 B), channels open through a voltage-independent reaction that can occur when the voltage sensor is either in its resting state ($C_R \leftrightarrow O_R$) or its activated state ($C_A \leftrightarrow O_A$). Importantly, the opening reaction is allosterically coupled to voltage sensor movement so that opening is much more favorable once the voltage sensor has activated. In response to a hyperpolarization from a holding potential where the voltage sensors are initially in the resting state, channels will therefore open along the $C_R \rightarrow C_A \rightarrow O_A$ pathway since the $C_R \rightarrow O_R$ opening reaction is energetically unfavorable.

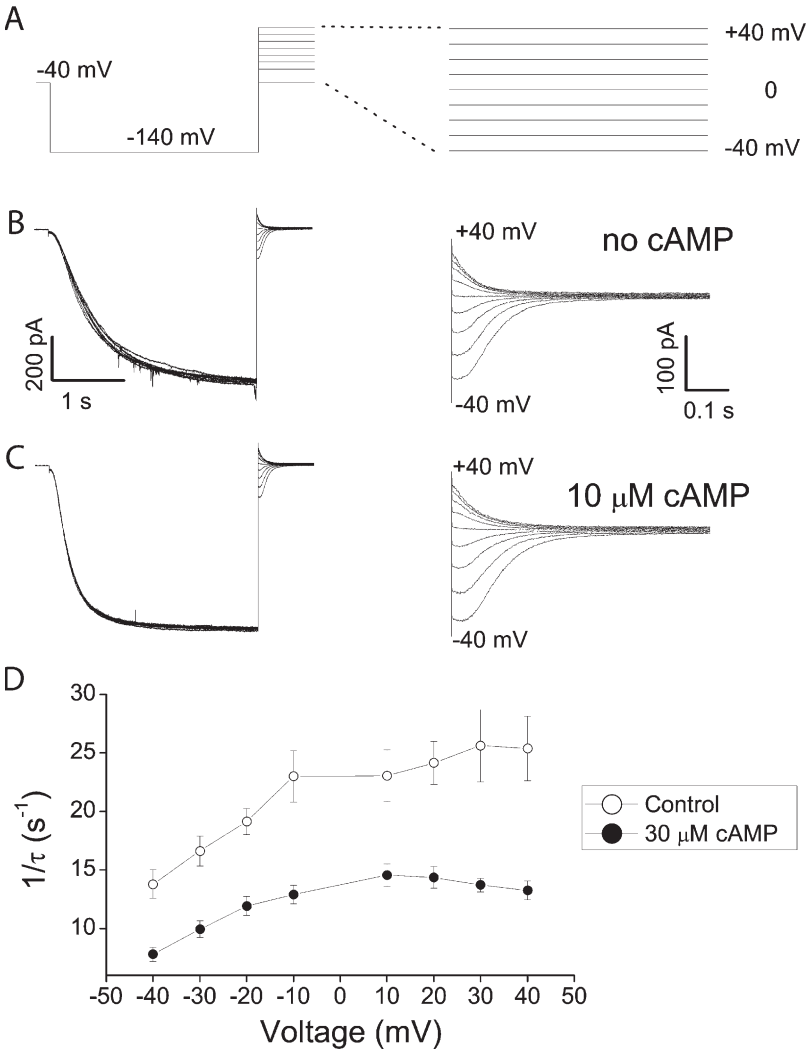

Figure 7. Effect of voltage and cAMP on HCN2 tail current kinetics. (A) Illustration of voltage pulse protocol. Membrane was held at −40 mV, stepped to −140 mV for 3 s, and then stepped to a series of more positive potentials to measure tail currents. Left, entire time course of protocol. Right, protocol on an expanded time scale during tail current measurements. Time scales are shown in B. (B) HCN2 currents in absence of cAMP, at either a slow time scale showing the entire time course during opening and closing protocols (left) or an expanded time scale illustrating tail currents (right). (C) Currents obtained in presence of 10 μM cAMP at a slow (left) and expanded (right) time scale. (D) Plot of $1/\tau$ for tail current decay (obtained from single exponential fits) as a function of voltage during tail current measurements, either in absence (open circles) or presence (filled circles) of cAMP. Bars show SE ($n = 4$).

Upon return to more positive voltages, channels will close through the $O_A \rightarrow O_R \rightarrow C_R$ pathway since the $O_R \rightarrow C_R$ closing transition is more energetically favorable than the $O_A \rightarrow C_A$ transition. Thus, the maximal, voltage-independent rate of closing determined from the tail current decay will largely reflect the voltage-independent, $O_R \rightarrow C_R$ reaction, which is more rapid than the $O_A \rightarrow C_A$ reaction because the O_R state is much less stable than the O_A state.

We first fit the four-state scheme to our HCN2 kinetic data obtained in the absence of cAMP. As shown in Fig. 8 B, the four-state scheme provides a reasonable description of both opening and tail current kinetics of HCN2 (Fig. 8 B). In particular, the simulated tail currents now decay with a similar time course to the experimental traces. In addition, similar to the experimental traces, the tail currents from the model show a characteristic lag or plateau upon steps to less depolarized potentials that is due to the fact that the closing reaction has to proceed through two sequential open states ($O_A \rightarrow O_R \rightarrow C_R$).

Is the cyclic allosteric scheme also consistent with the regulatory effects of cAMP on channel kinetics? To address this question we assumed that cAMP can bind to all four states of the channel and that all kinetic parameters of the voltage-dependent activation reactions and voltage-independent closed−open reactions can be modified by cAMP binding. This leads to an eight-state cubic scheme in which the four unliganded states of the channel form the vertices of the front face of the cube and the four cAMP-bound states form the vertices of the back face of the cube (Fig. 1 B; see Materials and methods). However, because our data were obtained either in the absence of cAMP (where channels can only occupy the four unliganded states) or in the presence of a saturating concentration of cAMP (where channels can only occupy the four cAMP-bound states), we can ignore all cAMP binding or unbinding transitions and fit our data in the absence or presence of cAMP separately using two appropriate four-state schemes.

As shown in Fig. 8 C, a fit of the four-state cyclic scheme is also able to provide a reasonable description

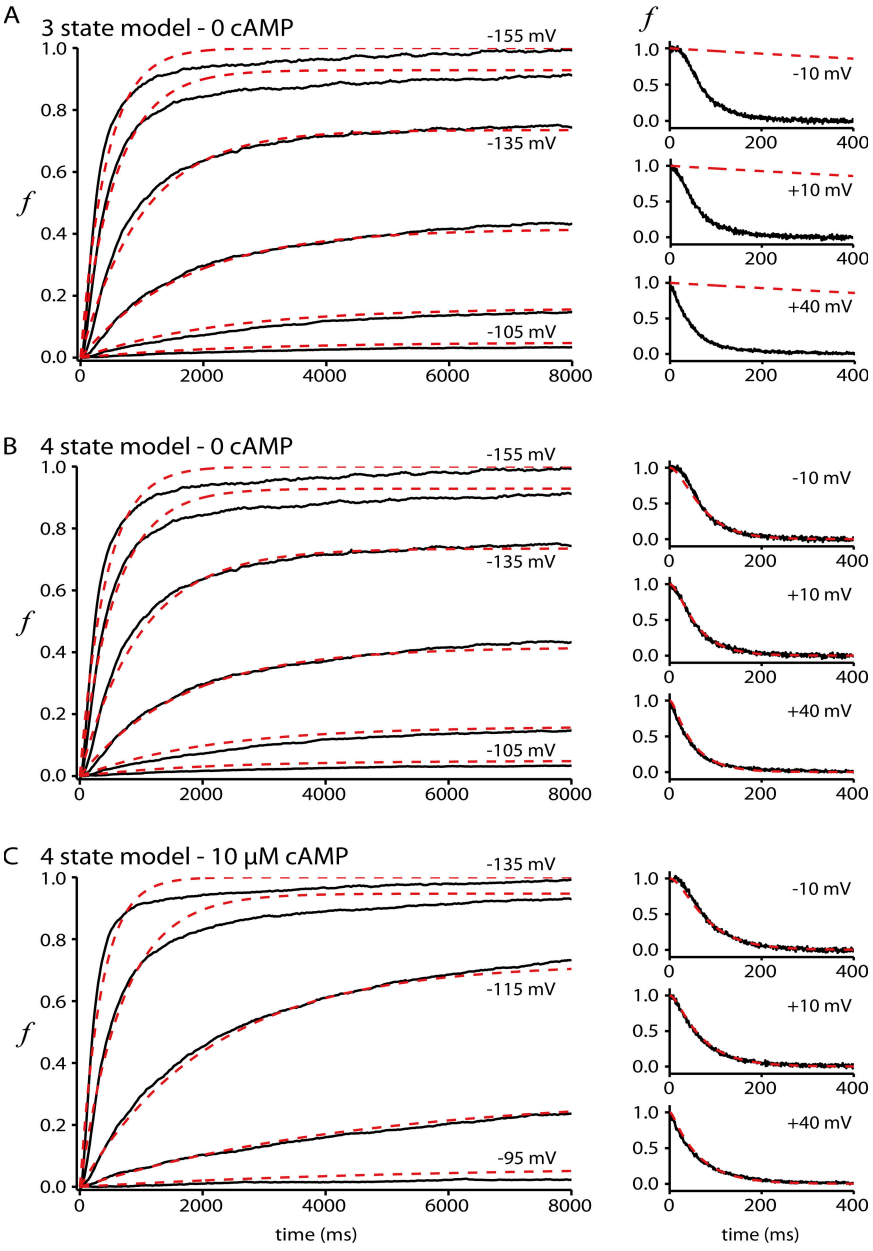

Figure 8. Fits of three-state and four-state gating schemes to HCN2 opening and closing kinetics. (A) Fits of the three-state scheme to normalized HCN2 currents in absence of cAMP. Left, HCN2 currents were measured in response to hyperpolarizing steps (10 s) from a holding potential of −40 mV to a series of test voltages in 10-mV increments (selected voltages indicated next to traces). Currents were converted to normalized open probabilities, $f(t)$, shown as solid black traces (see Materials and methods). Dashed red traces show best fit of three-state model to data. Only the first 8 s of each trace are shown. Right, HCN2 tail currents obtained at different depolarized potentials (shown next to traces) following steps to −140 mV to open the channels. Tail currents were converted to normalized open probabilities (solid black traces). Predictions of three-state model shown as dashed red traces. Best-fit parameters with their lower and upper limits (see Materials and methods) were as follows: $\alpha_0 = 3.2 \times 10^{-6}$, range from 1.2×10^{-7} to 8.0×10^{-5} ms^{-1}; s_α = 9.1, range from 8.0 to 11.6 mV; $\beta_0 = 415.8$, range from 18 to 7,500 ms^{-1}, $s_\beta = 49.0$, range is greater than 10.8 mV; $g = 0.0024$, range from 0.0016 to 0.004 ms^{-1}, $h = 3.8 \times 10^{-4}$, range from 2.7 to 5.7×10^{-4} ms^{-1}. See text for definition of parameters and Materials and methods for normalization procedure. The mean summed square error during fits is 0.0032 for current opening data and 5.0 for tail current data. (B) Fits of the four-state scheme to normalized HCN2 currents in absence of cAMP. Data and traces as in A. Best-fit parameters for the scheme are given in Table I. Note that the model provides a reasonable fit to both opening (left) and closing (right) kinetics. (C) Fits of four-state scheme to normalized HCN2 currents obtained in presence of 10 µM cAMP. The model again provides a reasonable description of both opening and closing kinetics. Because of the cyclic nature of the scheme, the rate constant α' (V) in fits of four-state schemes in B and C was calculated from the other rate constants to conform to microscopic reversibility.

of the HCN2 opening and closing kinetics in the presence of cAMP (Fig. 8 C), further supporting the model. A comparison of the parameter values for the fits of the four-state scheme in the absence and presence of cAMP reveals cAMP-dependent changes in all rate constants, including an increase in the voltage-independent opening rate and a decrease in the closing rate (Table I; four-state scheme, 10 µM cAMP). The latter results are consistent with our experimental observations that cAMP binding alters the maximal rates of channel opening and closing. A more stringent model in which cAMP binding selectively alters the rate constants of the voltage-independent closed–open transitions was also found to provide a reasonable fit to the data (Fig. S1, available at http://www.jgp.org/cgi/content/full/jgp.200609585/DC1). These modeling results are consistent with the view that the voltage-independent closed–open transition is subject to dual allosteric regulation by voltage sensor movement and cAMP binding.

DISCUSSION

Our experiments yield several insights into the mechanism by which HCN channel gating is dually regulated by voltage and cyclic nucleotide. First, we provide direct evidence for a voltage-independent kinetic step that limits the rate of opening and closing of HCN2. Although we do not detect a limit in the rate of HCN1 opening, the high sequence identity of the HCN channels makes it likely that HCN1 undergoes a similar voltage-independent closed–open transition. We presume that this voltage-independent opening step fails to become rate limiting for HCN1 because its opening kinetics are much faster than those of HCN2. Second, we show that the S4–S6 region is largely responsible for differences in the voltage-independent opening kinetics between the two channels. Third, we find that HCN2 kinetics can be described by an eight- state cyclic allosteric model in which a voltage-independent closed–open reaction is under dual allosteric control by voltage sensor movement and cAMP binding. These results confirm and extend previous studies on HCN channel gating (DiFrancesco, 1999; Altomare et al., 2001; Wang et al., 2002; Craven and Zagotta, 2004). They also reveal a strong similarity between the gating of HCN channels and the dual allosteric gating by voltage and Ca^{2+} of BK Ca^{2+}-activated K^+ channels (Horrigan and Aldrich, 2002).

Allosteric Mechanism of Voltage Gating for HCN Channels

Our finding of a maximal, voltage-independent limit in the rate of HCN2 channel opening led us to consider several models of channel gating. Such behavior is inconsistent with a simple two-state, closed–open reaction scheme in which the opening and closing rate constants exhibit a monotonic increase or decrease, respectively, with increasing hyperpolarization. Although it is possible to explain the voltage-independent kinetics by a two-state scheme if the rate constants of opening and closing exhibit saturating behavior at both extreme positive and negative voltages, such a two-state scheme is unable to explain the nonexponential delays in the time course of HCN2 opening and closing. Moreover, cAMP binding would need to alter the voltage dependence of the opening and closing rate constants in an arbitrary and complex manner to account for the effects of ligand on channel kinetics and open probability. In contrast, schemes in which channels undergo a well-behaved voltage-dependent activation reaction and a separate voltage-independent closed–open transition that is regulated by cAMP binding provide a simple and concise means of describing channel kinetics. Such models have previously been used both to explain the ability of cAMP to enhance the maximal open probability at negative voltages (Craven and Zagotta, 2004; Shin et al., 2004) and to account for the inhibitory action of general anesthetics to suppress the opening of HCN2 and HCN1 (Chen et al., 2005).

Although a three-state scheme is consistent with the channel opening kinetics, to account for the relatively rapid HCN2 tail current kinetics we needed to adopt a four-state cyclic model in which a voltage-independent closed–open reaction is allosterically coupled to a voltage-dependent activation reaction (Fig. 1 A). Finally, to explain the regulation of channel opening by both voltage and cAMP we expanded the four-state cyclic scheme into an eight-state cubic model, in which the closed–open transition was under dual allosteric regulation by voltage sensor movement and ligand binding (Fig. 1 B). However, even the eight-state model is an oversimplification of the true gating scheme since it fails to account for the extent of the sigmoidal delay in opening and closing kinetics at some potentials. To describe such delays, Altomare et al. (2001) used an allosteric gating scheme in which the closed–open transition was regulated by a Hodgkin-Huxley–like activation scheme involving the independent movement of four voltage sensors (although in the Altomare et al. model the closed–open transitions were voltage dependent and the effects of cAMP were not examined). We have chosen to use a simpler scheme with fewer free parameters to permit an objective fit of the model to our data in both the absence and presence of cAMP. Nonetheless, due to the simplifications of our model, it is important for us to distinguish conclusions that are model dependent from those that are model independent.

First, the voltage-independent limit in the rate of tail current decay demonstrates that the rate constant for the closing reaction ($O \rightarrow C$) must be voltage independent. This rules out all models in which the transitions among closed states (e.g., $C_R \leftrightarrow C_A$) or among open states (e.g., $O_R \leftrightarrow O_A$) are the voltage-independent ones whereas the open–closed reactions are voltage dependent. Moreover, the finding that cAMP increases the maximal open probability at extreme negative potentials (Shin et al., 2004; Craven and Zagotta, 2004) strongly argues that both the opening ($C \rightarrow O$) and closing ($O \rightarrow C$) transitions must be voltage independent, otherwise the channel should be able to be fully opened by strong hyperpolarization in the absence of cAMP.

Second, the ability of cAMP to enhance maximal open probability also implies that the voltage-independent opening and/or closing rates must be regulated by cAMP. Our finding that cAMP slows the voltage-independent rate of tail current decay provides direct evidence that the closing rate is modulated by cAMP. Our finding that cAMP also enhances the voltage-independent, maximal rate of channel opening supports the idea that this ligand also directly accelerates the opening reaction. However, because channel opening is preceded by more than one closed state, our results do not rule out more complex schemes in which both voltage-dependent and

voltage-independent transitions are permitted among multiple closed states (although our results do require that any closed–open reaction be voltage independent). Nonetheless, the eight-state cyclic allosteric scheme in which a voltage-independent opening reaction is dually regulated by cAMP binding and voltage sensor movement provides a minimally concise model for HCN channel gating.

Structural Basis for Allosteric Regulation of Channel Opening

Our chimera experiments identify distinct regions of HCN1 and HCN2 that independently regulate the voltage-independent closed–open transition and the voltage-dependent activation reaction. Thus, exchange of the C-terminal domains between HCN1 and HCN2 shifts the voltage dependence of channel opening kinetics by 10–20 mV, similar to the effect of these C-terminal regions on the voltage dependence of steady-state opening (Wang et al., 2001). In contrast, the S1–S6 transmembrane domain, and the S4–S6 region in particular, regulates the voltage-independent opening rate. An involvement of the S4–S6 region in regulating the opening reaction is consistent with the finding that the S6 segment forms the gate of the HCN channels (Rothberg et al., 2002) and that the S4–S5 loop communicates S4 voltage sensor movement to the S6 gate (Decher et al., 2004; Long et al., 2005).

Although the amino acid sequences of HCN1 and HCN2 differ at only 19 out of the 160 positions in the S4–S6 region, we have not been able to identify specific residues that are responsible for the kinetic differences between HCN1 and HCN2. Rather our mutagenesis results suggest that critical residues may be distributed throughout this region (unpublished data). Because the S4 segment is completely conserved between the two channels and there is only one conservative substitution in the S4–S5 loop, the key residues responsible for the kinetic phenotypes are likely to lie in the S5–S6 region that forms the channel pore and gate.

Potential Physiological Implications

What might be the potential physiological relevance of the voltage-independent kinetics of opening and closing? We found that the rate of opening of HCN2 begins to saturate at voltages ~20 mV negative to the midpoint voltage of gating. Although the midpoint voltage of activation is quite negative in cell-free patches due to a shift in gating upon patch excision (Pian et al., 2006), in intact cells the midpoint voltage of activation of I_h is as positive as −55 mV, suggesting that the rate of opening could approach its limiting value at physiologically relevant voltages.

HCN2 makes an important contribution to I_h in many cell types, including cardiac ventricular myocytes (Shi et al., 1999) and thalamic relay neurons (Ludwig et al., 2003), where I_h can contribute to spontaneous pacemaker activity. A limit to the rate of opening of HCN2 could ensure that there is a limit to the rate of spontaneous firing in these cells at extreme negative potentials, achieved, for example, during intense inhibitory input associated with thalamic spindling activity during slow wave sleep (Luthi and McCormick, 1998). HCN channels are also present in neurons that are not spontaneously active. In such cells, HCN channels contribute to the resting integrative properties of the neuron that shape the time course of an excitatory postsynaptic potential (EPSP) (Robinson and Siegelbaum, 2003). A limit in the rate of channel closing at depolarized voltages may allow HCN channels to differentially alter the magnitude and time course of a single EPSP, which may be too brief for channels to completely close, compared with a short burst of EPSPs, whose longer duration may permit full HCN channel closure. The function of these voltage-independent kinetics may be revealed in the future through detailed computer modeling or through the rescue of an HCN2 knockout mouse (Ludwig et al., 2003) with our HCN2/HCN1 212 chimera that exhibits a large enhancement in its voltage-independent opening rate.

We thank Dr. Edgar Young for helpful comments on an earlier version of the manuscript and Eric Odell for help with preparation of the figures. We also thank Anthony DeCostanzo and Huan Yao for help with generating constructs and John Riley for expert technical assistance.

This work was supported by grant NS36658 from the National Institutes of Health, the Howard Hughes Medical Institute, and the M.D.-Ph.D. program of Columbia University (M.S. George).

Olaf S. Andersen served as editor.

Submitted: 25 May 2006
Accepted: 10 January 2007

REFERENCES

Altomare, C., A. Bucchi, E. Camatini, M. Baruscotti, C. Viscomi, A. Moroni, and D. DiFrancesco. 2001. Integrated allosteric model of voltage gating of HCN channels. *J. Gen. Physiol.* 117:519–532.

Baruscotti, M., A. Bucchi, and D. Difrancesco. 2005. Physiology and pharmacology of the cardiac pacemaker ("funny") current. *Pharmacol. Ther.* 107:59–79.

Bell, D.C., H. Yao, R.C. Saenger, J.H. Riley, and S.A. Siegelbaum. 2004. Changes in local S4 environment provide a voltage-sensing mechanism for mammalian hyperpolarization-activated HCN channels. *J. Gen. Physiol.* 123:5–19.

Biel, M., A. Schneider, and C. Wahl. 2002. Cardiac HCN channels: structure, function, and modulation. *Trends Cardiovasc. Med.* 12:206–212.

Chen, J., J.S. Mitcheson, M. Lin, and M.C. Sanguinetti. 2000. Functional roles of charged residues in the putative voltage sensor of the HCN2 pacemaker channel. *J. Biol. Chem.* 275:36465–36471.

Chen, X., J.E. Sirois, Q. Lei, E.M. Talley, C. Lynch III, and D.A. Bayliss. 2005. HCN subunit-specific and cAMP-modulated effects of anesthetics on neuronal pacemaker currents. *J. Neurosci.* 25:5803–5814.

Chen, S., J. Wang, and S.A. Siegelbaum. 2001. Properties of hyperpolarization-activated pacemaker current defined by coassembly of HCN1 and HCN2 subunits and basal modulation by cyclic nucleotide. *J. Gen. Physiol.* 117:491–503.

Craven, K.B., and W.N. Zagotta. 2004. Salt bridges and gating in the COOH-terminal region of HCN2 and CNGA1 channels. *J. Gen. Physiol.* 124:663–677.

Decher, N., J. Chen, and M.C. Sanguinetti. 2004. Voltage-dependent gating of hyperpolarization-activated, cyclic nucleotide-gated pacemaker channels: molecular coupling between the S4-S5 and C-linkers. *J. Biol. Chem.* 279:13859–13865.

DiFrancesco, D. 1999. Dual allosteric modulation of pacemaker (f) channels by cAMP and voltage in rabbit SA node. *J. Physiol.* 515:367–376.

DiFrancesco, D., and P. Tortora. 1991. Direct activation of cardiac pacemaker channels by intracellular cyclic AMP. *Nature.* 351:145–147.

Goulding, E.H., J. Ngai, R.H. Kramer, S. Colicos, R. Axel, S.A. Siegelbaum, and A. Chess. 1992. Molecular cloning and single-channel properties of the cyclic nucleotide-gated channel from catfish olfactory neurons. *Neuron.* 8:45–58.

Hille, B. 2001. Ion Channels of Excitable Membranes. Sinauer Associates, Inc., Sunderland, MA. 325–326.

Hodgkin, A.L., and A.F. Huxley. 1952. A quantitative description of membrane current and its application to conduction and excitation in nerve. *J. Physiol.* 117:500–544.

Horrigan, F.T., and R.W. Aldrich. 2002. Coupling between voltage sensor activation, Ca^{2+} binding and channel opening in large conductance (BK) potassium channels. *J. Gen. Physiol.* 120:267–305. (published erratum appears in *J. Gen. Physiol.* 2002. 120:599.)

Ishii, T.M., M. Takano, and H. Ohmori. 2001. Determinants of activation kinetics in mammalian hyperpolarization-activated cation channels. *J. Physiol.* 537:93–100.

Long, S.B., E.B. Campbell, and R. Mackinnon. 2005. Voltage sensor of Kv1.2: structural basis of electromechanical coupling. *Science.* 309:903–908.

Ludwig, A., X. Zong, M. Jeglitsch, F. Hofmann, and M. Biel. 1998. A family of hyperpolarization-activated mammalian cation channels. *Nature.* 393:587–591.

Ludwig, A., T. Budde, J. Stieber, S. Moosmang, C. Wahl, K. Holthoff, A. Langebartels, C. Wotjak, T. Munsch, X. Zong, et al. 2003. Absence epilepsy and sinus dysrhythmia in mice lacking the pacemaker channel HCN2. *EMBO J.* 22:216–224.

Luthi, A., and D.A. McCormick. 1998. H-current properties of a neuronal and network pacemaker. *Neuron.* 21:9–12.

Mannikko, R., F. Elinder, and H.P. Larsson. 2002. Voltage-sensing mechanism is conserved among ion channels gated by opposite voltages. *Nature.* 419:837–841.

Mannikko, R., S. Pandey, H.P. Larsson, and F. Elinder. 2005. Hysteresis in the voltage dependence of HCN channels: conversion between two modes affects pacemaker properties. *J. Gen. Physiol.* 125:305–326.

Pian, P., A. Bucchi, R.B. Robinson, and S.A. Siegelbaum. 2006. Regulation of gating and rundown of HCN hyperpolarization-activated channels by exogenous and endogenous PIP2. *J. Gen. Physiol.* 128:593–604.

Press, W.H., S.A. Teukolsky, W.T. Vetterling, and B.P. Flannery. 1992. Numerical Recipes in C. Second edition. Cambridge University Press, New York. 656–706.

Robinson, R.B., and S.A. Siegelbaum. 2003. Hyperpolarization-activated cation currents: from molecules to physiological function. *Annu. Rev. Physiol.* 65:453–480.

Rothberg, B.S., K.S. Shin, P.S. Phale, and G. Yellen. 2002. Voltage-controlled gating at the intracellular entrance to a hyperpolarization-activated cation channel. *J. Gen. Physiol.* 119:83–91.

Santoro, B., D.T. Liu, H. Yao, D. Bartsch, E.R. Kandel, S.A. Siegelbaum, and G.R. Tibbs. 1998. Identification of a gene encoding a hyperpolarization-activated pacemaker channel of brain. *Cell.* 93:717–729.

Santoro, B., S. Chen, A. Luthi, P. Pavlidis, G.P. Shumyatsky, G.R. Tibbs, and S.A. Siegelbaum. 2000. Molecular and functional heterogeneity of hyperpolarization-activated pacemaker channels in the mouse CNS. *J. Neurosci.* 20:5264–5275.

Shi, W., R. Wymore, H. Yu, J. Wu, R.T. Wymore, Z. Pan, R.B. Robinson, J.E. Dixon, D. McKinnon, and I.S. Cohen. 1999. Distribution and prevalence of hyperpolarization-activated cation channel (HCN) mRNA expression in cardiac tissues. *Circ. Res.* 85:e1–e6.

Shin, K.S., C. Maertens, C. Proenza, B.S. Rothberg, and G. Yellen. 2004. Inactivation in HCN channels results from reclosure of the activation gate: desensitization to voltage. *Neuron.* 41:737–744.

Stieber, J., A. Thomer, B. Much, A. Schneider, M. Biel, and F. Hofmann. 2003. Molecular basis for the different activation kinetics of the pacemaker channels HCN2 and HCN4. *J. Biol. Chem.* 278:33672–33680.

Vaca, L., J. Stieber, X. Zong, A. Ludwig, F. Hofmann, and M. Biel. 2000. Mutations in the S4 domain of a pacemaker channel alter its voltage dependence. *FEBS Lett.* 479:35–40.

Vemana, S., S. Pandey, and H.P. Larsson. 2004. S4 movement in a mammalian HCN channel. *J. Gen. Physiol.* 123:21–32.

Viscomi, C., C. Altomare, A. Bucchi, E. Camatini, M. Baruscotti, A. Moroni, and D. DiFrancesco. 2001. C terminus-mediated control of voltage and cAMP gating of hyperpolarization-activated cyclic nucleotide-gated channels. *J. Biol. Chem.* 276: 29930–29934.

Wainger, B.J., M. DeGennaro, B. Santoro, S.A. Siegelbaum, and G.R. Tibbs. 2001. Molecular mechanism of cAMP modulation of HCN pacemaker channels. *Nature.* 411:805–810.

Wang, J., S. Chen, and S.A. Siegelbaum. 2001. Regulation of hyperpolarization-activated HCN channel gating and cAMP modulation due to interactions of COOH terminus and core transmembrane regions. *J. Gen. Physiol.* 118:237–250.

Wang, J., S. Chen, M.F. Nolan, and S.A. Siegelbaum. 2002. Activity-dependent regulation of HCN pacemaker channels by cyclic AMP: signaling through dynamic allosteric coupling. *Neuron.* 36:451–461.

Zagotta, W.N., N.B. Olivier, K.D. Black, E.C. Young, R. Olson, and E. Gouaux. 2003. Structural basis for modulation and agonist specificity of HCN pacemaker channels. *Nature.* 425:200–205.